Patch-Based Nonlinear Image Registration for Gigapixel Whole Slide Images

J. Lotz*, J. Olesch, B. Müller, T. Polzin, P. Galuschka, J. M. Lotz, S. Heldmann, H. Laue, M. González-Vallinas, A. Warth, B. Lahrmann, N. Grabe, O. Sedlaczek, K. Breuhahn, and J. Modersitzki

Abstract—*Objective*: Image registration of whole slide histology images allows the fusion of fine-grained information—like different immunohistochemical stains—from neighboring tissue slides. Traditionally, pathologists fuse this information by looking subsequently at one slide at a time. If the slides are digitized and accurately aligned at cell level, automatic analysis can be used to ease the pathologist's work. However, the size of those images exceeds the memory capacity of regular computers. *Methods*: We address the challenge to combine a global motion model that takes the physical cutting process of the tissue into account with image data that is not simultaneously globally available. Typical approaches either reduce the amount of data to be processed or partition the data into smaller chunks to be processed separately. Our novel method first registers the complete images on a low resolution with a nonlinear deformation model and later refines this result on patches by using a second nonlinear registration on each patch. Finally, the deformations computed on all patches are combined by interpolation to form one globally smooth nonlinear deformation. The NGF distance measure is used to handle multistain images. *Results*: The method is applied to ten whole slide image pairs of human lung cancer data. The alignment of 85 corresponding structures is measured by comparing manual segmentations from neighboring slides. Their offset improves significantly, by at least 15%, compared to the low-resolution nonlinear registration. *Conclusion/Significance*: The proposed method significantly improves the accuracy of multistain registration which allows us to compare different antibodies at cell level.

Index Terms—Computer-aided diagnosis, digital pathology, histopathology, image registration.

I. INTRODUCTION: HIGH-RESOLUTION HISTOLOGICAL WHOLE SLIDE IMAGING

IN cancer diagnostics and histology-related basic research, much insight into molecular and cellular interactions, tissue growth, and tissue organization is gained by analyzing consecutive and differently stained histological sections. For this procedure, a fixed tissue is transferred in a paraffin block and cut into 2–5 μm thin slices, stained by, e.g., immunohistochemistry, and subsequently examined by a scientist or physician using conventional or virtual microscopy.

In order to correlate the staining intensity, staining patterns, and even subcellular localization of different proteins or antigens, costaining is frequently required. However, the detection of different antigens is usually difficult due to crossreactivity of primary and secondary antibodies used for the staining process [1]. Adjacent serial sections can be used to separate crossreacting chemicals, by staining them separately, resulting in two or more images, one for each antibody. To recombine the information from the separate stains, a precise, multimodal image registration is essential.

When dealing with histological whole slide images, an important challenge is the size of these images. At its maximum resolution, a whole slide image often exceeds the size of 100 000 × 100 000 pixels. Established registration methods cannot process data at this resolution without being adapted for special high-performance computing hardware.

However, high-power magnification and especially the adjustment of staining information derived from different slides are of central importance for basic research and for medical diagnostics. For example, an integrated picture containing morphological and partly subcellular features (e.g., the nuclear shape) together with the expression of specific tumor cell markers is necessary for reliable diagnosis of some solid tumor. Moreover, combining staining patterns from adjacent sections may allow the mapping of protein expression to specific cell populations in tissues consisting of multiple cell populations.

Next to the accurate alignment of corresponding tissue structures, the regularity and reliability of the deformation is crucial to the quality of a registration result. In the process of cutting sections from a block, different artifacts can occur [2]. Some of these deformations, such as tissue compression, have an influence on large parts of the tissue slide. To undo such a deformation, a model that globally couples all parts of the tissue seems appropriate. Common choices are diffusive [3], elastic [4], or curvature-based deformation models [5].

The global coupling of the deformation leads to a dilemma when facing patch-based registration methods as the image information is not globally available at a high resolution.

Previous work dealing with the registration of such images focuses either on a nonlinear registration of low-resolution images [6]–[8] or approaches the problem with patch-based methods where smaller patches of the image are registered affinely [7], [9], [10]. While being considerably faster, low-resolution approaches cannot take local deformations into account. These deformations are invisible without using the full-resolution data. Patch-based methods that rely on a combination of affine or rigid registrations are limited in the number of degrees of freedom.

We present a novel method that first registers the complete images on a low resolution and later refines this result on patches by using a second nonlinear registration on each patch. Finally, the deformations computed on all patches are combined by interpolation to form one globally smooth nonlinear deformation. This approach combines global deformation information on a coarse level with a local correction.

We organize the rest of this paper as follows: related work dealing with the registration of histology images will be discussed in Section II. We then demonstrate the challenges a registration approach has to deal with when it comes to histology images in Section III. The core of the presented method is the nonlinear, variational registration approach [11]. The relevant parts with respect to the computational challenges on large images will be discussed in Section IV. Our extension, a patch-based nonlinear registration method, will be presented in Section IV-E. We apply the new method to human lung cancer data, as described in Section V, and present an evaluation of the results in Section VI. In the end, we discuss merits and shortcomings of the presented method.

II. RELATED WORK

Digital pathology is an active topic of research. Most of the work in this field dealing with image registration focuses on 3-D reconstruction which usually includes multiple image registrations of consecutive histologic slides. This paper focuses on the core of these methods, the registration of two consecutive slides.

Starting back in the 90s, the first methods were established to reconstruct digitized histological data to 3-D volumes mostly for a better anatomical understanding of specific organs. Many papers formulate the goal to reconstruct 2-D histological images to 3-D volumes and fuse them to corresponding 3-D volumes of another modality, e.g., MRI or PET scans [12], [13], block-face images [14]–[17] or both [18], [19]. For this aim, every 2-D histological slide is aligned with a corresponding slide of the reference volume. As the reference volumes are of limited image resolution, the used resolutions of the histological slide images are also low.

A different kind of method solves the problem without a reference volume. For low-resolution 3-D reconstructions from histological data, an affine or rigid registration of two or more consecutive slides is satisfying [16], [20]–[24]. More complex deformation models allow a more accurate alignment. Examples include piecewise or weighted affine deformations [10], [25], [26], b-spline deformations [6], [7], [27], a moving least squares

approach applied to SIFT points [28] and elastic registration [29].

Today, advanced imaging technology results on the one hand in much higher amounts of data and on the other hand in a shift of reconstruction tasks. One example is the growing interest in the reconstruction of global or functional entities such as microvasculature or immunohistochemical markers [7]. The new challenge is to reconstruct and fuse the data on a completely different level: smaller structures and the comparison of different functional markers across slides are of increasing interest, resulting in the need of reconstructions ideally on the scale of cell nuclei. For this task, affine or rigid solutions are not sufficient. Nonlinear deformations that occur in the cutting process have to be corrected to achieve satisfying results.

Even though the performance of the technology to compute histological reconstructions has advanced significantly, the high amount of histological data cannot be handled with the classical established methods on common workstation computers. This even holds true for the data needed to fulfill only a subset of the 3-D reconstruction task, the registration of two successive slides. There are different approaches to address the challenge of the large image dimensions.

In the following, we distinguish between global methods that compute a solution based on extracted features or another subset of the data on one hand and those methods that implement a divide and conquer approach on the other. Global detection of the cell nuclei is used by Weiss *et al.* [30] to reduce the tissue data to nuclei densities that can be stored efficiently due to the sparsity of the nuclei. These densities are independent of a particular staining and are used to compute a global deformation of whole slide images.

Schwier *et al.* [8] reduce the image data to segmented vessel structures to steer their two-step approach. First a rigid, iterative best-fit matching of the segmented vessel structures is calculated which is refined by an elastic registration step on a low-resolution image. The resulting deformation is then applied to the original slice data.

By matching SIFT features, Cardona *et al.* [28] register images from transmission electron microscopy (TEM). Patches captured from TEM are stitched in plane while they are reconstructed in 3-D at the same time. Using SIFT point correspondences as distance measure, they combine rigid and nonlinear deformation components by a moving least squares approach [31].

Instead of reducing the amount of data and possibly losing important detail information, local methods divide the image into smaller parts and process these parts independently. One advantage of such an approach is that well-established registration methods can be used. One big interest in these methods is the way the individually computed results are combined into one final deformation.

The idea of transforming selected image regions affinely is followed in [25]. Arsigny *et al.* compute a global, poly-affine registration by combining multiple affine transformations while maintaining smoothness at the tile borders. However, because of the simultaneous computation of multiple regions, the method is not meant to work with large images. Using nonrectangular patches, Pitiot *et al.* [10] propose a registration framework,

where automatically segmented partitions of the images are generated based on tissue structure such as the gyri of the brain. The regions are transformed independently by an affine registration. A global transformation is then found by interpolating the transformation between the registered partitions.

Closest to our new method is the work of Song *et al.* [9] on 3-D tissue reconstruction of histological sections that are differently stained. The authors propose a tile-based approach previously published by Roberts *et al.* [7] that first computes a rough globally rigid transformation which is then refined by calculating rigid transformations on smaller patches of the image with higher resolution. Multimodal registration between differently stained sections is achieved by an automated content classification. A global nonlinear deformation is computed by interpolating between rigidly transformed points on individual patches using b-spline transformations.

In the sectioning process, physical forces are exerted and propagated globally through the tissue. Compared to the aforementioned approaches, we use a physically motivated nonlinear transformation model (such as diffusive, elastic, or curvature registration) on the entire domain of the whole slide image. In previous experiments [32], we used a zooming strategy to compute a high-resolution registration of a successively decreasing image area. We extend this strategy by switching completely to nonlinear registrations and by performing multiple registrations on overlapping image regions. The resulting deformation vector fields are finally combined to produce one large, smooth nonlinear deformation.

III. COMPUTATIONAL CHALLENGES IN DIGITAL PATHOLOGY

The challenges in the registration of large images become apparent in the following example. To compute the transformation y^* that aligns two images R and T, we consider a registration framework that implements the variational scheme [11] such as described in the pseudo-code below

```
y^0 = affine_pre_registration(R,T)
J(R,T,y) = distance(R,T(y))
            + regularizer(y)
loop until stoppingCriteriaMet:
  compute J(R,T,y^i), ∇J(R,T,y^i)
  y^{i+1} = compute_update(J,∇J,y^i)
  i = i + 1
end
y* = y^i
```

The details will be covered in Section IV.

The loop is usually embedded in a multilevel or coarse-to-fine approach in order to convexify the registration problem and to prevent the registration from converging to a local minimum. In order to exploit the complete image information, gray values at every pixel are accessed multiple times during the optimization to compute the image gradient and the distance measure. As loading this data from the disk is slow, the images, the image gradient, and the transformation are usually kept in the computer's main memory.
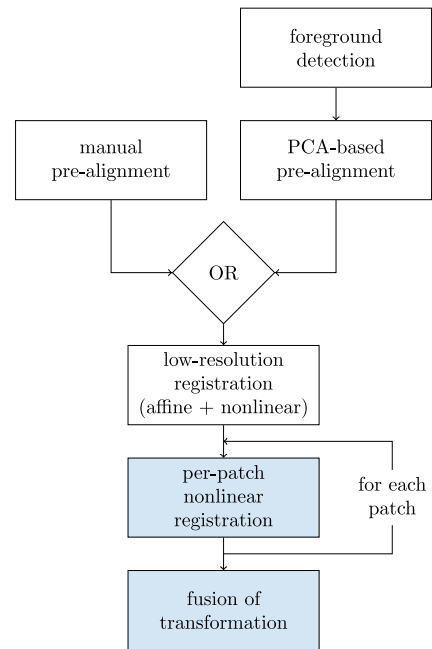

Fig. 1. Registration scheme for two histology whole slide images. We focus on patch-based registration and fusion of the deformation.

The sizes of image and image gradient provide a lower bound to the main memory required by the registration algorithm. Typical whole slide images in digital pathology are scanned with a magnification referred to as 40× (typically 0.228 μm × 0.228 μm per pixel) and have dimensions of 100 000 × 100 000 = 10^{10} pixels or even more. If converted to grayscale images and stored in double precision (64 bit/pixel = 8 byte/pixel), one such image requires $8 \cdot 10^{10}$ byte = 76 294 MB = 74.51 GB of main memory. Even at the slightly lower magnification of 20× (0.455 μm × 0.455 μm per pixel), which seems sufficient for registration purposes, one image still sums up to 18.63 GB. Considering both images and the derivative of the template image, the total memory requirement for the registration is at least 75 GB. Often, the deformation information can be stored on a lower resolution, therefore, we neglect it in this calculation. Further, we do not include any other variables such as intermediate deformed images or other temporary computation results.

With the intended use on a regular desktop workstation or laptop computer in mind, these requirements excess the available resources of rarely more than 32 GB of main memory.

This problem has been addressed by processing the image in patches as noted in Section II. We extend this idea and propose a novel method where a physically motivated, nonlinear registration is computed first globally and then corrected locally on each patch. After all patches are registered, the resulting deformation fields are combined into one smooth deformation.

IV. METHODS: NONLINEAR IMAGE REGISTRATION

The main methodological contribution of this paper is in the patch-based nonlinear registration. This registration is preceded by an initial alignment that will be discussed first. Fig. 1 shows an overview of the different components of the proposed automatic registration scheme.

A. Prealignment

To initialize the registration, the slices are prealigned by the following steps:

1. Normalize the image intensities.
2. Identify the foreground of the image by variance filtering and thresholding.
3. Align the image by their principal axes [33].
4. Refine the alignment by an affine image registration of the masks computed in 2.) using the SSD distance measure [11].

A similar strategy has recently been used by [6] and others. The result of the prealignment is used as an initial guess to start the actual registration.

B. Nonlinear Image Registration

The core of the patch-wise registration is the image registration method described in [11]. We understand image registration as the computation of a deformation $y : \mathbb{R}^2 \to \mathbb{R}^2$ that maps from a reference coordinate frame, defined on a reference image R onto the coordinate frame of the template image T. Using an efficient, matrix-free implementation [34] of the variational approach, the functional

$$J[y] = D[T, R, y] + S[y] \longrightarrow \min$$

is optimized with respect to a deformation y. D and S represent a distance measure and a regularizer.

To cope with the multimodality of differently stained image sections, we choose the normalized gradient field (NGF) [35] distance measure

$$D[T, R, y] = \text{NGF}[T, R, y]$$
$$= \int_\Omega 1 - \left(\frac{\nabla T(y(x))^T \nabla R(x)}{||\nabla T(y(x))||_\varepsilon \, ||\nabla R(x)||_\varepsilon} \right)^2 \, \mathrm{d}x$$

where $||x||_\varepsilon^2 = ||x||_2^2 + \varepsilon^2$ to assess image similarity. By aligning normalized image gradients, NGF not only allows the registration of differently stained images but also copes nicely with different staining intensities in same-stain (monomodal) registration.

The histological cutting process exerts forces to the tissue block that we want to model physically. As a tradeoff between accurate modeling and computation speed, we choose a diffusive regularizer [3]

$$S[y] = \frac{\alpha}{2} \int_\Omega \langle \nabla y(x), \nabla y(x) \rangle \, \mathrm{d}x$$

which can be interpreted as a special case of the linear elasticity [4].

C. Efficiently Discretizing the Deformation

We represent the deformation on the reference image's domain by a deformed grid $\mathbf{y} \in \mathbb{R}^{m \times n \times 2}$ of size $m \times n$ where

$$\mathbf{y} = \mathbf{x} + \mathbf{u}$$

is a combination of a regular, cell-centered grid $\mathbf{x} = h \cdot [0.5, 1.5, \ldots, m - h/2] \times h \cdot [0.5, 1.5, \ldots, n - h/2]$ with spacing h and a displacement $\mathbf{u}$ relative to the grid. By using regularization, we can assume that the deformation is smooth in

the sense that local variations are small. For this reason, its resolution can be much lower than the number of pixels in the image without loosing much information. Intermediate positions are interpolated. We chose the deformation resolution $m \times n$ to be one to two orders of magnitude lower (in each dimension) than the number of pixels in the image. The low amount of data needed to store the deformation significantly lowers the memory requirements and runtime of the registration and makes it possible to handle the global deformation for the whole slide image. This is reflected in the implementation as shown in the following paragraphs.

The image T is a representation of the underlying image data which is obtained by linear interpolation. The reference image $\mathbf{R}$ is defined on its regular pixel grid $\mathbf{X} \in \mathbb{R}^{M \times N \times 2}$ of size $M \times N (> m \times n)$.

In this context, the expression $\sum_{\hat{x} \in \mathbf{X}}$ in (1) is meant as the sum over all grid points $\hat{x} \in \mathbb{R}^2$ of the grid $\mathbf{X}$ and can be thought of as a for-loop. Furthermore, in a discrete setting, $\bar{\nabla}$ is meant as a finite difference operator.

The objective function with respect to the discretized deformation can then be written as

$$\min_{\mathbf{u}} \, J[T, \mathbf{R}, \mathbf{y}] = \mathbf{D}[T, \mathbf{R}, P\mathbf{y}] + \mathbf{S}[\mathbf{u}], \text{where}$$

$$\mathbf{u} = \mathbf{y} - \mathbf{x},$$

$$\mathbf{D}[T, \mathbf{R}, P\mathbf{y}] = \mathbf{NGF}[T, \mathbf{R}, P\mathbf{y}]$$

$$= h^2 \cdot \sum_{\hat{x} \in \mathbf{X}} 1 - \left(\frac{\bar{\nabla} T(P\mathbf{y}[\hat{x}])^T \bar{\nabla} \mathbf{R}(\hat{x})}{||\bar{\nabla} T(P\mathbf{y}[\hat{x}])||_\varepsilon \, ||\bar{\nabla} \mathbf{R}(\hat{x})||_\varepsilon} \right)^2$$

$$\mathbf{S}[\mathbf{u}] = \frac{\alpha}{2} \sum_{\hat{u} \in \mathbf{u}} \langle \bar{\nabla} \hat{u}, \bar{\nabla} \hat{u} \rangle \qquad (1)$$

and P is the prolongation operator which interpolates the low-resolution deformation onto the image grid $\mathbf{X}$. The square brackets in the expression $y[x]$ denote the bilinear interpolation of $\mathbf{y}$ based on the four neighboring pixels of $\mathbf{x}$ on the grid of $\mathbf{y}$.

D. Optimization

The optimization of the objective function is embedded in a multilevel coarse-to-fine approach that avoids local minima by starting the registration with a smoothed image. The image's resolution is then subsequently increased to account for details in the images. This method has been described multiple times, see, e.g., [11] for more details.

As optimizer, an L-BFGS [36] implementation is used that is initialized with the analytic Hessian of the regularizer.

An affine preregistration is used to compute a rough alignment of the two images that is used as an initial guess for the deformation y.

E. Patch-Based Image Registration

As described in Section III, it is not practical to use the above framework to compute a registration of two whole slide images due to the large amount of data. In contrast to earlier patch-based linear registration methods, our method computes the registration in two steps which are both nonlinear and which allows a free choice of the deformation model.

By computing a first nonlinear registration on low-resolution data, global large-scale deformations occurring in the tissue are corrected. The result of this nonlinear registration is then used as initial guess for a patch-wise registration scheme.

1) Patchwise Elastic Registration: After computing the registration on the low-resolution data, the image is partitioned into patches. The patches are allowed to overlap. A high-resolution correction of the first deformation is computed independently on each patch by means of a second nonlinear registration. At this high resolution, smaller structures are visible and drive the registration process such that local deformations of the tissue slides are compensated. Each local registration returns a vector field with the computed transformation.

The algorithm is described formally in the following pseudo-code. The global domain Ω of the reference image is defined as a rectangular region $\Omega = [\omega^{11}, \omega^{12}] \times [\omega^{21}, \omega^{22}] \subset \mathbb{R}^2$ in the world coordinate system of the reference object slide. The image deformation in this domain is represented by a discrete deformation field $\mathbf{y}$ which is defined as an array of dimensions $m \times n$ and is coupled to a world matrix W. Multiplication of W with homogeneous pixel coordinates transforms these coordinates into the world coordinate system of Ω. Each patch is defined on a domain $\Omega_{j,k} \subset \Omega$ and a deformation $\mathbf{y}_{j,k}$ is computed.

```
compute Ω_{j,k}, W_{j,k} for all patches in Ω
for j = 1:M_patches:
    for k = 1:N_patches:
        y_{j,k} = minimize J(R, T, y)|_{Ω_{j,k}}
    end
end
```

This results in the computation of $M_{\text{patches}} \cdot N_{\text{patches}}$ deformations.

2) Fusion of Deformations $\mathbf{y}_{j,k}$: In order to obtain a global smooth deformation $y_\Omega(x)$ on the original image domain Ω, bilinear interpolation is used. We first consider the 1-D problem of fusing the patches in one column. The following step will be repeated for all columns k, $k = 1, \ldots, N_{\text{patches}}$.

If the coordinate x in the global deformation y_Ω is only covered by one patch, say patch (j, k), the value at this point can be obtained from the deformation $y_{j,k}$ by interpolation. Note that the square brackets in the expression $y[x]$ again denote bilinear interpolation

$$y_\Omega(x) = y_{(j,k)}[W_{j,k}^{-1} W_\Omega x]$$

$$\text{if } W_\Omega x \in \Omega_{j,k}.$$

If a point in y is covered by two patches, we interpolate linearly and obtain $y_\Omega(x)$ by

$$y_\Omega(x) = d(x) \quad \cdot \quad y_{(j,k)}[W_{j,k}^{-1} W_\Omega x]$$
$$+ (1 - d(x)) \quad \cdot \quad y_{(j+1,k)}[W_{j+1,k}^{-1} W_\Omega x]$$
$$\text{if } W_\Omega x \in \Omega_{j,k} \cap \Omega_{j+1,k}$$

where $d(x) = (x^{(1)} - \omega^{11}_{j+1,k})/(\omega^{12}_{j,k} - \omega^{11}_{j+1,k})$ is the relative distance of x to the border of patch $j + 1, k$. Note that $\omega^{12}_{j,k} - \omega^{11}_{j+1,k} > 0$ because the patches are overlapping.

The global smoothness of the fused deformation, is assured by comparing the two norm of the differences of the deformation vectors in the overlapping region $||y_{(j,k)}[W_{j,k}^{-1} W_\Omega x] - y_{(j+1,k)}[W_{j+1,k}^{-1} W_\Omega x]||_2^2$. In the course of the experiments, the difference between neighboring patches was always lower than 5%.

All patches are aligned in rows and columns such that we can first apply the above method to fuse each column of patches and then use the same method again on the resulting row.

The core registration component is implemented in a C++ library with focus on efficiency and shared-memory parallelization [34]. The preprocessing and the patch-based registration are assembled in the image processing framework MeVisLab. The algorithm used to fuse the deformation was implemented in the Julia programming language and will be made publicly available.

V. APPLICATION TO HUMAN LUNG CANCER DATA

As a proof of principle, we applied the patch-based nonlinear registration method to a clinically relevant question: human lung cancer. Nonsmall cell lung cancer with its two subtypes adenocarcinoma and squamous cell carcinoma (SCC) is the most common cause of cancer-related death worldwide [37]. Morphological features such as the nuclear morphology as well as the expression of marker gene panel (e.g., cytokeratins) are informative for the characterization of tumor cell dedifferentiation. We therefore decided to use a primary SCC isolated from a human lung cancer patient.[1] See the appendix for detailed information about the staining process.

The algorithm was run on ten independent slide pairs with stains CD31 - H&E (2 pairs), H&E - Factor VIII, Factor VIII - KL1, KL1 - CD31, CD146 - KL1 (4 pairs), CD146 - AFOG (13 different slides in total, see Table I). The patch size can be chosen depending on the memory capacity of the computer at hand. We found a patch size of 4096×4096 pixels to work well on a laptop computer equipped with 16 GB of RAM and an Intel i7 processor. Patches were overlapping by 20% on each border. The number of patches per image depend on the image's size at the desired magnification level. To trade-of visible detail and computation time, we choose a magnification of $20\times$ (0.455 μm $\times$ 0.455 μm per pixel) for all images. This results in a number of patches between $3 \times 7 = 21$ and $13 \times 17 = 221$ patches per image. See Table I for an overview of the data used for the evaluation.

The NGF distance measure was parametrized with $\varepsilon = 10\,000$, the regularization parameter was set to $\alpha = 0.1$.

VI. VALIDATION

The evaluation of the accuracy of a registration in general is a difficult task and it is even more difficult if no ground truth or gold standard is available. In application to histology data,

TABLE I
OVERVIEW OF THE IMAGE DATA USED FOR EVALUATION

dataset ID	stainings	image dimensions	# patches
L0-1	CD31 - H&E	R: 55680×46592 + T: 59520×45568	63
L0-2	H&E - F. VIII	R: 59520×45568 T: 55552×46720 +	198
L0-3	F. VIII - KL1	R: 55552×46720 + T: 57536×44672 +	221
L0-4	KL1 - CD31	R: 57536×44672 + T: 55552×51982 +	206
L0-5	CD31 - H&E	R: 55552×51982 + T: 56580×46592	209
L1-1	CD146 - KL1	R: 35712×29344 + T: 31744×24960 +	28
L1-2	KL1 - CD146	R: 31744×24960 + T: 35712×31744 +	21
L1-3	CD146 - KL1	R: 35712×31744 + T: 23558×17280 +	35
L1-4	KL1 - CD146	R: 23558×17280 + T: 23808×17280 +	28
K1-1	CD146 - AFOG	R: 43648×43136 + T: 41664×40192 +	49

The algorithm has been evaluated on ten slide pairs and six different stains. All slides were registered with the spatial resolution of 0.455 μm $\times$ 0.455 μm per pixel. A plus (+) denotes that the image resolution is given after downsampling to 0.455 μm by a factor of 2 in each dimension.

Fig. 2. LEFT: Two independent annotations of the same structure with representative inaccuracies, $d_{\max} = 11.4$ μm, $d_{\text{avg}} = 1.8$ μm. RIGHT: Registration result, template image with transformed contour from reference image, $d_{\max} = 10.1$ μm, $d_{\text{avg}} = 2.5$ μm. The black bar has a length of 200 μm.

such as for example in 3-D reconstruction, an exact match of corresponding structures is usually not even desired, as it would annihilate the structural differences present in two neighboring slides, and thus, destroy the 3-D structure. In the case of virtual double staining, 3-D structure is not of primary interest, still, an objective ground truth is not available. In [24], this problem is addressed by comparing automatically detected nuclei-landmarks. However, detection of such nuclei correspondences is difficult in multistain data. Accepting a possible bias in favor of an intensity-based registration, we chose to manually segment larger structures that are identifiable in both slides.

The accuracy of the registration is evaluated by computing the differences of manual segmentations of corresponding structures after registration. A similar evaluation has been used in [9]. In each slide pair, 5–12 structures were segmented manually without knowledge of the registration result. Each segmentation is represented by approximately 200–400 points.

For each two segmentations, represented by point sets $A = \{a_1, \ldots, a_N\}$ and $B = \{b_1, \ldots, b_M\}$, the maximum $d_{\max}$ and mean offset d_{avg} between the corresponding structures was computed with

$$d_{\max} = \max \left\{ \max_{a \in A} \min_{b \in B} \|a - b\|_2 \,,\, \max_{b \in B} \min_{a \in A} \|b - a\|_2 \right\}$$

and

$$d_{\text{avg}} = \max \left\{ \operatorname*{avg}_{a \in A} \min_{b \in B} \|a - b\|_2 \,,\, \operatorname*{avg}_{b \in B} \min_{a \in A} \|b - a\|_2 \right\}.$$

The maximum distance is known as the discrete Hausdorff distance [38] and has been previously used to evaluate histology registrations [9]. The mean distance between the annotations is
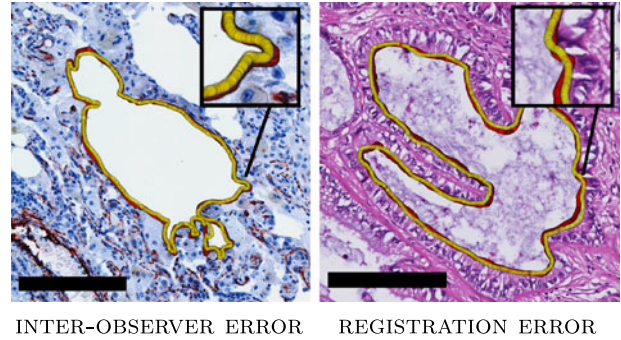
less sensitive toward outliers in the manual annotations, and is therefore, included in the validation.

To estimate the interobserver error while drawing the segmentations, 12 annotations of one slide have been drawn twice. The measured values for maximum and mean distance between the segmentations is $\text{avg}(d_{\max}) = 15.1 \pm 11.9$ μm and $\text{avg}(d_{\text{avg}}) = 2.3 \pm 0.7$ μm which serves as an approximation of the lowest measurable registration error. Fig. 2 shows one of these segmentations (left) and also a pair of segmentations after registration (right).

Distances were computed after PCA-prealignment, after low-resolution nonlinear registration and after the patch-based registration. The results for each slide pair are reported in Table II. The results show that the nonlinear preregistration is an efficient method to obtain a relatively accurate result if processing time is the priority. However, after the additional correction using the patch-based method, the distances between the structures are lower in all cases. The overall reduction is 15% for the Hausdorff distance and 36% for the mean segmentation distance. The final registration error is in the order of magnitude of the accuracy of the manual segmentations.

A one-sided paired t-test was computed with the null-hypothesis that the new method is not better than the coarse-level registration. The hypothesis was rejected, both improvements are statistically significant ($p < 0.025$). As two metrics were used to compare the registration accuracy, the significance level was adjusted using the Bonferroni correction.

The additional quality becomes also apparent if the results are evaluated visually. One example is shown in Fig. 3, where the alignment of the structures using the patch-based method is almost at cell-level accuracy while a significantly larger registration error is visible in the low-resolution registration. See the attached movie for an illustration of the virtual double staining process based on the registration result.

Comparing the registration accuracy to other methods such as [9], [7], [10] is difficult due to the lack of a common benchmark and freely available data. This remains true, even in the cases where a comparable error measure has been used. While the registration error shown above seems to be lower than in the results reported by [9], tissue properties such as slice thickness and tissue deformations have a big influence on the quality of the

TABLE II
MAXIMUM SEGMENTATION OFFSET (DISCRETE HAUSDORFF DISTANCE, TOP) AND MEAN SEGMENTATION OFFSET (BOTTOM) AFTER PCA-BASED PREALIGNMENT, AFTER LOW-RESOLUTION NONLINEAR REGISTRATION AND AFTER PATCH-BASED REGISTRATION ON TEN EVALUATED SLIDE PAIRS

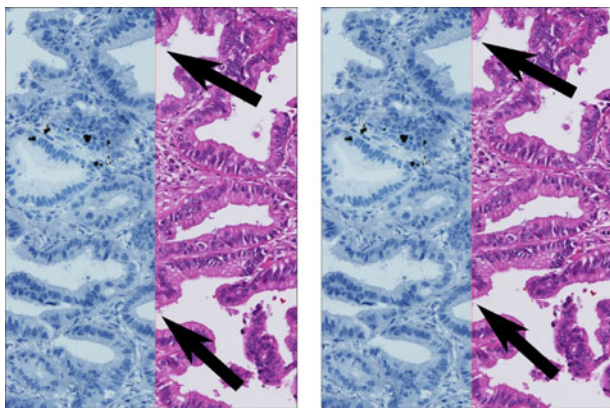| Maximum segmentation offset d_{max} (discrete Hausdorff distance)			
dataset ID (# segmentations)	pre aligned	low resolution	patch based
L0-1 (5)	126.4 μm	21.1 μm	**15.9 μm**
L0-2 (6)	178.5 μm	20.8 μm	**12.6 μm**
L0-3 (6)	126.4 μm	18.6 μm	**11.0 μm**
L0-4 (6)	186.1 μm	21.0 μm	**13.0 μm**
L0-5 (6)	543.8 μm	22.8 μm	**12.7 μm**
L1-1 (12)	44.7 μm	18.7 μm	**16.4 μm**
L1-2 (11)	42.2 μm	18.6 μm	**18.0 μm**
L1-3 (11)	64.3 μm	19.9 μm	**19.1 μm**
L1-4 (10)	94.4 μm	35.2 μm	**33.6 μm**
K1-1 (12)	39.0 μm	26.8 μm	**26.4 μm**
average (85)	122 μm	22.7 μm	**19.3 μm**
Mean segmentation offset d_{avg}			
dataset ID (# segmentations)	pre aligned	low resolution	patch based
L0-1 (5)	47.1 μm	8.7 μm	**3.4 μm**
L0-2 (6)	118.4 μm	9.1 μm	**4.9 μm**
L0-3 (6)	47.1 μm	6.3 μm	**3.6 μm**
L0-4 (6)	129.4 μm	7.8 μm	**3.5 μm**
L0-5 (6)	455.8 μm	10.7 μm	**3.4 μm**
L1-1 (12)	15.4 μm	4.9 μm	**3.6 μm**
L1-2 (11)	19.1 μm	4.1 μm	**3.5 μm**
L1-3 (11)	26.0 μm	5.2 μm	**3.6 μm**
L1-4 (10)	49.3 μm	4.8 μm	**3.5 μm**
K1-1 (12)	14.6 μm	5.8 μm	**5.8 μm**
average (85)	79.0 μm	6.1 μm	**3.9 μm**

Fig. 3. Comparison of low-resolution (LEFT) and patch-based (RIGHT) registration results on tissue stained with H&E and CD31. Smoother structure correspondence is seen in the results generated with the new method.

registration and a fair comparison is not possible. To facilitate future comparisons, the data and the segmentations used for the evaluation in this paper have been made available.[2]

The present implementation is meant as a proof of concept and has not been optimized for performance. Naturally, the large amount of data in the whole slide images increases the computation time. The average runtime of the algorithm is 49 s

for the nonlinear preregistration (exclusive of prealignment) and between 22 min (24 patches) and 288 min (206 patches) for the patch-based correction. The fusion of the deformation of 206 patches is computed in less than 30 s.

VII. CONCLUSION

In registration of histology data, image size is an important issue as one slide can have an amount of data surpassing the equivalent of 30 CT images. When dealing with nonlinear registration, a global deformation is modeled and the deformation in one point of the image domain has a global influence on the image. This leads to the dilemma where a global deformation needs to be computed but the data cannot be handled globally at the necessary resolution.

We propose a two-stage solution to this problem. First, a low-resolution global nonlinear registration is computed that accounts for the low-frequency, global deformation of the tissue. This registration is later corrected for the high-frequency local parts of the deformation which are invisible at low-resolution representations of the images. We chose a simple approach computing the registration independently for each patch. This approach already results in a significant improvement compared to the low-resolution registration. One downside is the significantly longer runtime which is unavoidable due to the larger amount of data that is processed. However, the method has the potential to be easily parallelization on multiple machines as no communication between the processes that align the patches is necessary. An interesting extension of the method is in the use of the information from those patches that are already computed when computing the high-resolution patches. This however, poses new questions on the order in which patches should be computed and is postponed to future work.

VIII. ATTACHED MULTIMEDIA FILE

As a proof of concept, the attached movie[3] demonstrates the virtual double staining using the proposed patch-based registration method. The initially shown AFOG stain is registered to a slide stained with CD146. Stained epithelial structures are highlighted in orange and transferred to the AFOG stain where the two stains can now be analyzed simultaneously.

APPENDIX
HISTOLOGY STAINING PROTOCOL

In brief, after fixation of a tissue slice (about 7 cm × 5 cm × 0.5 cm) in 4 % buffered formalin over night, the tissue was cut in smaller pieces (about 1 cm × 1 cm), transferred in paraffin, and systematically cut in 1-2 μm thick sections using a conventional microtome. Afterwards, five consecutive sections were stained using hematoxylin/eosin (H&E) and acid fuchsin orange G (AFOG) standard protocols. In addition, the following antibodies were used for epitope-specific stains: anti-CD31/PECAM1 (clone MEC13.3, BD Biosciences, Heidelberg, Germany), anti-CD146/MCAM (polyclonal, Atlas Antibodies, Stockholm, Sweden), Factor VIII light chain antibody (clone H-100, Santa Cruz Biotechnology, Heidelberg, Germany, and an

[2]http://s.fhg.de/histo-registration-data

[3]The movie is also available here: http://s.fhg.de/rg-dbl-stn.

anti-pan cytokeratin antibody (clone KL1, Abcam, Cambridge, UK). Staining was performed using the Dako Autostainer (Hamburg, Germany) and the following protocol: tissue slides were air-dried in an incubator at $42°$ C over night and deparaffinized in xylene (2×10 min). After rehydration in graded ethanol, the slides were pretreated in 0.01 M sodium citrate (pH 6.0) in a pressure cooker for 10 min. Afterwards, primary antibodies in PBS/Tween were added for 30 min at room temperature and slides were washed with PBS/Tween for 5 min before the secondary antibody was applied for 20 min (1:1.000 in PBS/Tween). The samples were then incubated with 1% hydrogen peroxide diluted in PBS/Tween (5 min). After signal detection using amino-ethyl-carbazol (AEC, 2×7 min) nuclei were stained using haematoxylin.

REFERENCES

[1] I. B. Buchwalow and W. Böcker, *Immunohistochemistry: Basics and Methods*. New York, NY, USA: Springer, 2010.

[2] V. Rastogi, "Artefacts: A Diagnostic Dilemma A Review," *J. Clin. Diagnostic Res.*, vol. 7, no. 10, pp. 2408–2413, 2013.

[3] J. Modersitzki and B. Fischer, "Fast diffusion registration," in *Proc. Contemporary Math.*, 2000, vol. 313, pp. 117–127.

[4] C. Broit, "Optimal registration of deformed images," Ph.D. dissertation, Dept. Comput. Inf. Sci., Univ. Pennsylvania, Philadelphia, PA, USA, 1981.

[5] B. Fischer and J. Modersitzki, "Curvature based image registration," *J. Math. Imag. Vis.*, vol. 18, pp. 81–85, 2003.

[6] M. Feuerstein *et al.*, "Reconstruction of 3-D histology images by simultaneous deformable registration," in *Proc. Med. Image Comput. Comput.-Assisted Intervention*, Jan. 2011, vol. 14, pp. 582–589.

[7] N. Roberts *et al.*, "Toward routine use of 3D histopathology as a research tool," *Amer. J. Pathol.*, vol. 180, no. 5, pp. 1835–1842, May 2012.

[8] M. Schwier *et al.*, "Registration of histological whole slide images guided by vessel structures," *J. Pathol. Informat.*, vol. 4, no. 10, 2013.

[9] Y. Song *et al.*, "Unsupervised content classification based nonrigid registration of differently stained histology images," *IEEE Trans. Biomed. Eng.*, vol. 61, no. 1, pp. 96–108, Jan. 2014.

[10] A. Pitiot *et al.*, "Piecewise affine registration of biological images for volume reconstruction," *Med. Image Anal.*, vol. 10, no. 3, pp. 465–483, Jun. 2006.

[11] J. Modersitzki, *FAIR: Flexible Algorithms for Image Registration*. Philadelphia, PA, USA: SIAM, 2009.

[12] M. S. Mega, "Mapping histology to metabolism: Coregistration of stained whole-brain sections to premortem PET in Alzheimer's disease," *NeuroImage*, vol. 5, no. 2, pp. 147–153, 1997.

[13] M. M. Chakravarty *et al.*, "The creation of a brain atlas for image guided neurosurgery using serial histological data," *NeuroImage*, vol. 30, no. 2, pp. 359–376, 2006.

[14] J. Dauguet *et al.*, "Three-dimensional reconstruction of stained histological slices and 3D non-linear registration with in-vivo MRI for whole baboon brain," *J. Neurosci. Methods*, vol. 164, no. 1, pp. 191–204, 2007.

[15] S. Gefen, "Elastic 3-D alignment of rat brain histological images," *IEEE Trans. Med. Imag.*, vol. 22, no. 11, pp. 1480–1489, Nov. 2003.

[16] E. Bardinet *et al.*, "Co-registration of histological, optical and MR data of the human brain," in *Proc. Med. Image Comput. Comput.-Assisted Intervention*, Sep. 2002, pp. 548–555.

[17] B. Kim *et al.*, "Mutual information for automated unwarping of rat brain autoradiographs," *NeuroImage*, vol. 5, no. 1, pp. 31–40, 1997.

[18] T. Schormann and K. Zilles, "Three-dimensional linear and nonlinear transformations: An integration of light microscopical and MRI data," *Human Brain Mapping*, vol. 6, nos. 5–6, pp. 339–347, 1998.

[19] E. Bardinet *et al.*, "Three dimensional functional cartography of the human basal ganglia by registration of optical and histological serial sections," in *Proc. IEEE Int. Symp. Bimed. Imag.*, 2002, pp. 329–332.

[20] L. Hibbard and R. Hawkins, "Objective image alignment for three-dimensional reconstruction of digital autoradiograms," *J. Neurosci. Methods*, vol. 26, no. 1, pp. 55–74, 1988.

[21] A. Andreasen *et al.*, "Computer-assisted alignment of standard serial sections without use of artificial landmarks. A practical approach to the utilization of incomplete information in 3-D reconstruction of the hippocampal region," *J. Neurosci. Methods*, vol. 45, no. 3, pp. 199–207, 1992.

[22] S. Ourselin *et al.*, "Reconstructing a 3D Structure from Serial Histological Sections," *Image Vis. Comput.*, vol. 19, nos. 1–2, pp. 25–31, Jan. 2001.

[23] G. Malandain, E. Bardinet, K. Nelissen, and W. Vanduffel, "Fusion of autoradiographs with an MR volume using 2-D and 3-D linear transformations," *NeuroImage*, vol. 23, no. 1, pp. 111–127, Sep. 2004.

[24] Y. Xu *et al.*, "A method for 3D histopathology reconstruction supporting mouse microvasculature analysis," *PloS One*, vol. 10, no. 5, Jan 2015.

[25] V. Arsigny *et al.*, "Polyrigid and polyaffine transformations: A novel geometrical tool to deal with non-rigid deformations—Application to the registration of histological slices," *Med. Image Anal.*, vol. 9, no. 6, pp. 507–523, Dec. 2005.

[26] K. Huang *et al.*, "Fast automatic registration algorithm for large microscopy images," in *Proc. IEEE/NLM Life Sci. Syst. Appl. Workshop*, 2006, pp. 1–2.

[27] T. Yunhao *et al.*, "Feature curve-guided volume reconstruction from 2D images," in *Proc. IEEE Int. Symp. Bimed. Imag.*, 2007, pp. 716–719.

[28] A. Cardona *et al.*, "An integrated micro- and macroarchitectural analysis of the Drosophila brain by computer-assisted serial section electron microscopy," *PLoS Biol.*, vol. 8, no. 10, Jan. 2010.

[29] O. Schmitt *et al.*, "Image registration of sectioned brains," *Int. J. Comput. Vis.*, vol. 73, no. 1, pp. 5–39, Sep. 2006.

[30] N. Weiss *et al.*, "Multimodal image registration in digital pathology using cell nuclei densities," in *Proc. Bildverarbeitung für die Medizin*, Mar. 2015, pp. 245–250.

[31] S. Schaefer *et al.*, "Image deformation using moving least squares," *ACM Trans. Graph.*, vol. 25, no. 3, pp. 533–540, 2006.

[32] J. Lotz *et al.*, "Zooming in: High resolution 3D reconstruction of differently stained histological whole slide images," *Proc. SPIE Med. Imag.: Digital Pathol.*, pp. 904104-1–904104-7, 2014.

[33] N. M. Alpert *et al.*, "The principal axes transformation—A method for image registration," *J. Nuclear Med.*, vol. 31, no. 10, pp. 1717–1722, 1990.

[34] L. König and J. Rühaak, "A fast and accurate parallel algorithm for nonlinear image registration using normalized gradient fields," in *Proc. IEEE Int. Symp. Bimed. Imag.*, Beijing, China, Apr. 2014, pp. 580–583.

[35] E. Haber and J. Modersitzki, "Intensity gradient based registration and fusion of multi-modal images," *Methods Inf. Med.*, vol. 46, no. 3, pp. 292–299, 2006.

[36] D. C. Liu and J. Nocedal, "On the limited memory BFGS method for large scale optimization," *Math. Programm.*, vol. 45, nos. 1–3d, pp. 503–528, 1989.

[37] J. R. Molina *et al.*, "Non-small cell lung cancer: Epidemiology, risk factors, treatment, and survivorship," *Mayo Clinic Proc.*, vol. 83, no. 5, pp. 584–594, 2008.

[38] D. Huttenlocher *et al.*, "Comparing images using the Hausdorff distance," *IEEE Trans. Pattern Anal. Mach. Intell.*, vol. 15, no. 9, pp. 850–863, Sep. 1993.

Authors' photographs and biographies not available at the time of publication.